

Copper-modified sulfated stannia: surface properties and catalytic activity towards phenol hydroxylation

Hussein A. Khalaf · Saber E. Mansour · Enas A. El-Madani

Received: 17 September 2009 / Accepted: 2 May 2010 / Published online: 3 June 2010
© Springer-Verlag 2010

Abstract Stannia, sulfated stannia, and Cu-modified sulfated stannia samples were prepared by an impregnation method using different loading levels of Cu (5, 10, and 20% by weight). These samples were characterized by means of thermal gravimetric analysis (TGA and DTA), X-ray powder diffraction (XRD), and nitrogen sorption at 77 K. Potentiometric titration was used to characterize the surface acidity of these samples and their catalytic activity was investigated by phenol hydroxylation in the presence of hydrogen peroxide at 333 K. The obtained data revealed sulfated species with different thermal stabilities in the samples containing Cu, and the rutile structure of stannia remained unchanged by the addition of sulfate and Cu. A surface texture study showed that Cu modification and the addition of sulfate resulted in modified surface area and porosity. The addition of copper to sulfated stannia increases the acid strength. Thus, Cu-modified sulfated stannia samples have higher catalytic activity towards phenol hydroxylation and selectivity towards hydroquinone production.

Keywords Stannia · Sulfation · Texture · Acidity · Phenol hydroxylation

Introduction

Porous solids with uniform pore size in the micropore and mesopore range are extensively used in industrial catalytic

processes. These materials possess high surface area, thermal stability, uniform pore structure, and tunable acid–base and redox properties. Chemical and physical properties of solid materials strongly depend on both the size and the shape of the microscopic particles they are made up from [1–3]. Modification of metal oxides with the sulfate anion can generate a strong acidity, even stronger than 100% sulfuric acid, and hence they become superacid catalysts useful in reactions like isomerizations, low temperature esterification, alkylation, and cracking [4, 5]. For sulfated metal oxides, the textural properties and catalytic activity can be improved by the addition of another metal component. Metal-promoted sulfated oxides are receiving increasing interest owing to their enhanced catalytic activity. The promoting effect of different metals like Mn, Fe, Ni, and Al on some metal oxides such as Fe_2O_3 and ZrO_2 has been reported [6, 7]. Since metal oxide systems containing tin oxide are widely used in oxidation reactions, it is expected that their sulfated analogues can show enhanced activity. Matsuhashi et al. [8] reported that the addition of sulfate anion to SnO_2 improves its oxidation activity in the dehydrogenation of cyclohexanol. Stannia-based catalysts exhibit good activity towards CO/O_2 and CO/NO reactions [9]. The activity and selectivity of stannia catalysts can be substantially improved by incorporation of heteroelements [10]. The copper ion and complexes containing copper ions have long been found to be effective catalysts and are used in a wide range of organic syntheses [11, 12]. Hydroxylation of phenols gives three different compounds, namely catechol, hydroquinone, and resorcinol. These phenolic derivatives are widely used as photography chemicals, antioxidants, polymerization inhibitors, and also in medicine [13].

Copper-containing porous materials appear to be promising catalysts for phenol hydroxylation with hydrogen

H. A. Khalaf (✉) · S. E. Mansour · E. A. El-Madani
Chemistry Department, Faculty of Science,
Omer El-Mukhtar University,
P.O. Box 919, El-Beida, Libya
e-mail: hkhalf70@yahoo.com

peroxide. However, little is known about the effect of the loading level of copper on catalyst activity and product distribution. In this work, we report the synthesis, bulk characterization, and acidic properties as well as catalytic behavior of Cu-modified sulfated stannia for the partial oxidation of phenol with H_2O_2 .

Results and discussion

Thermal analysis

From all prepared samples analyzed by thermal analysis, i.e., thermal gravimetric analysis (TGA) and differential thermal analysis (DTA), only four samples have been selected to be shown here. From the TG profile of the precursor tin gel ($SnO_2 \cdot xH_2O$; Fig. 1a), it can be seen that there are two mass loss steps in the temperature range room temperature (rt) to 1,273 K. The first step, which ends at 423 K with loss of mass of ~3.6% and is accompanied by an endothermic peak at 383 K, is attributed to the loss of volatile materials like physisorbed water [14]. The second one begins just after the first (683 K), bringing the mass loss to ~19.9%, and is assigned to dehydration processes (DTA exothermic peak at 643 K) [15, 16]. The theoretical mass loss of tin gel stoichiometrically approaching $SnO_2 \cdot 2H_2O$ to anhydrous SnO_2 is 19.3% (Scheme 1). The experimental mass loss is ~19.9% hence this implies that the tin gel sample approaches the suggested formula. Thus, the exhibited thermal events involve in general elimination of water bound with different strengths and a final formation of SnO_2 , which is well in agreement with the X-ray powder diffraction (XRD) data. The thermal behavior of stannia is still unchanged by the incorporation of copper (not shown). As to the sulfated sample 6STO, there are three mass loss steps (Fig. 1b). The first two steps, ending at 473 K (endothermic peak at 393 K) and 643 K (exothermic peak at 693 K), are attributed to removal of adsorbed water and the dehydration process of tin gel. The mass loss at higher temperature began at 973 K and ended at 1,053 K accompanied with an endothermic peak at 1,013 K. It was attributed to decomposition of sulfate groups [7, 17]. TGA and DTA for copper-modified sulfated stannia with loading level 20% by weight (20CuSTO) is shown in Fig. 1c. The obtained thermogram displays the same thermal events as the 6STO sample except that the mass loss due to sulfate decomposition appears at higher temperature in 20CuSTO (1,053–1,093 K) than in 6STO (993–1,053 K). Therefore, the presence of copper in sulfated stannia increased the stabilization of sulfate groups. These results are in agreement with the reported data [17, 18].

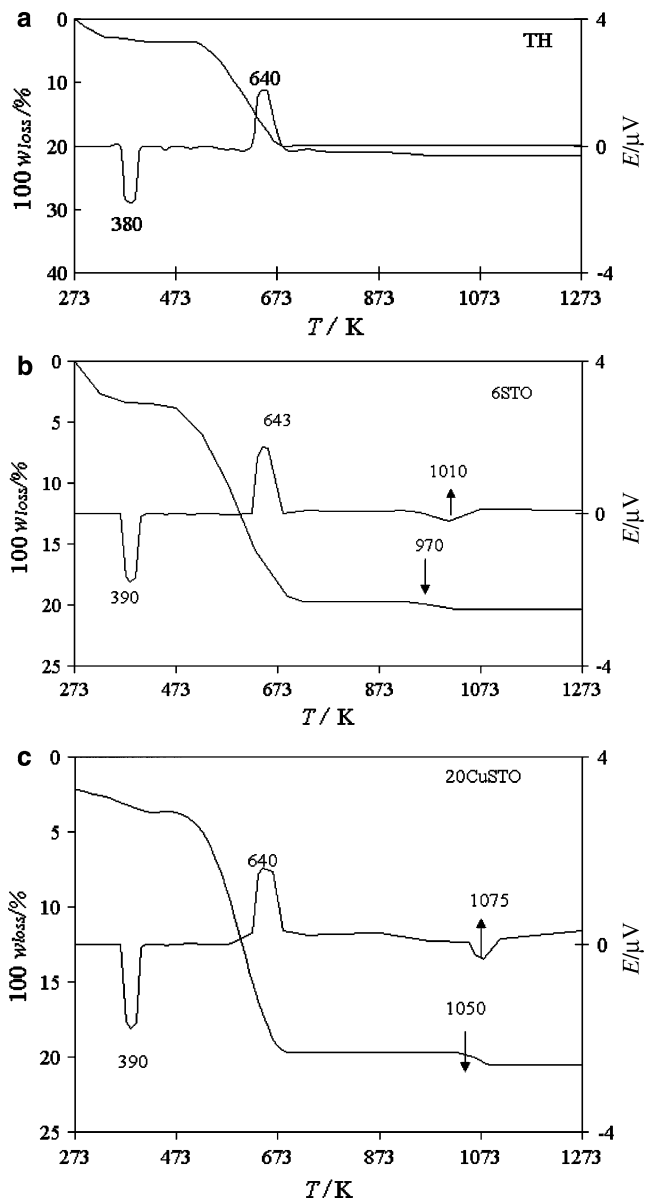


Fig. 1 TGA and DTA profiles for **a** stannia gel (TH), **b** sulfated stannia (6STO), **c** 20% Cu-modified sulfated stannia (20CuSTO); w_{loss} is the mass fraction



Scheme 1

X-ray diffraction

XRD patterns for pure and modified stannia samples (TO, $xCuTO$, 6STO, and $xCuSTO$) are shown in Fig. 2. From these XRD diffractograms and after matching the characteristic peaks with the relevant ASTM standards, it can be seen that all data point towards the rutile (tetragonal) SnO_2 phase (ASTM card No. 41-1445). The rutile structure has a

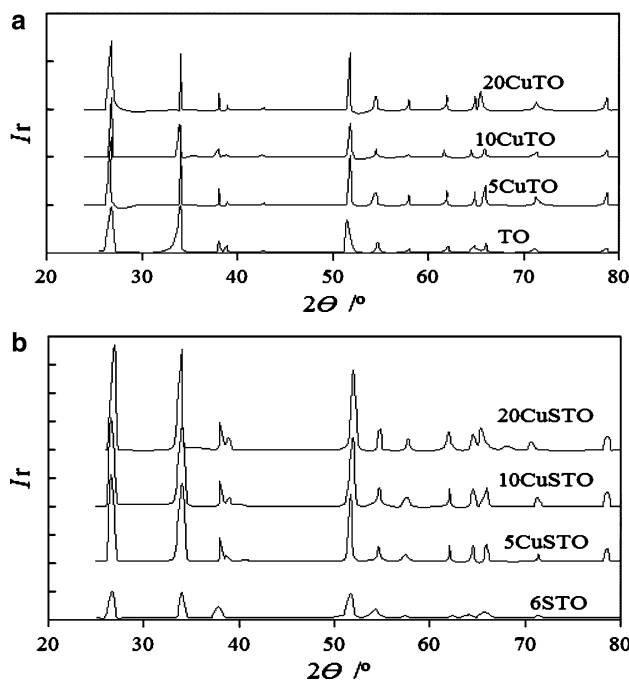


Fig. 2 X-ray powder diffractograms for **a** TO and x CuTO and **b** 6STO and x CuSTO catalysts; I_r is the relative intensity

tetragonal unit cell with lattice constants $a = b = 4.7374 \text{ \AA}$ and $c = 3.1864 \text{ \AA}$. In the bulk, all Sn atoms are sixfold coordinated to threefold coordinated oxygen atoms. The Scherrer equation was used, assuming a shape factor of 1.0 [19], to estimate average crystallite sizes of SnO_2 by using its (110) reflections. The crystallite sizes are shown in Table 1. The addition of Cu into stannia does not change

the crystal phase structure. This means that copper oxide is well dispersed on the support material. However, there is a slightly higher degree of crystallization after modification with Cu at the low loading level of 5%. This can be noticed from the higher peak intensities of this sample (5CuTO). After that, any increasing in the loading level of Cu resulted in a decrease in the degree of crystallization that can be noticed from the decreasing of peak intensities of the samples 10CuTO and 20CuTO. Jyothi et al. [4] found that the addition of a second oxide, e.g., La_2O_3 , CeO_2 , or Sm_2O_3 , to stannia hinders the crystallization of SnO_2 by preventing the aggregation of smaller particles. The addition of sulfate (Fig. 2b) was associated with a decrease in crystallite size to 88 Å, which may be attributed to the sulfate groups that remain bound at the surface of the samples and inhibit the growth of SnO_2 crystallites, agreeing thus with results obtained for other transition metal oxides, i.e., TiO_2 , ZrO_2 , and Fe_2O_3 [20]. The decrease in the crystallite size can be explained by the hypothesis that the bulky sulfate groups on the surface of SnO_2 particles prevent their agglomeration during calcination [21]. On the other hand, XRD patterns of x CuSTO samples (Fig. 2b) strongly suggested that the addition of Cu into SnO_2 followed by sulfation has no effect on the crystal phase of SnO_2 . There are little differences in the degree of crystallization for these samples compared with pure stannia and Cu-modified stannia. Thus, one can suggest that the addition of Cu into TO sample hinders the role of sulfate in crystal growth. The crystallite size for these samples ranges from 185 Å for 5CuSTO to 130 Å for 20CuSTO.

Table 1 Nitrogen sorption analysis data

Sample	S_{BET} ($\text{m}^2 \text{ g}^{-1}$)	C_{BET}	S_t^a ($\text{m}^2 \text{ g}^{-1}$)	S_s^b ($\text{m}^2 \text{ g}^{-1}$)	S_{cum}^c ($\text{m}^2 \text{ g}^{-1}$)	V_{Pcum}^d ($\text{cm}^3 \text{ g}^{-1}$)	V_{Ptot}^e ($\text{cm}^3 \text{ g}^{-1}$)	r_p^f (Å)	Crystallite size ^g (Å)	
TO	11		14.7	10.3	10.8	6.9	0.016	0.0325	17.5	185
5CuTO	11		3.4	9.7	11	4.0	0.006	0.0093	11.8	307
10CuTO	12		3.6	9.9	12.2	5.4	0.007	0.0108	12.2	177
20CuTO	14		3.1	13.2	14.5	6.1	0.008	0.0124	11.4	156
6STO	35		2.7	34	34.6	17.4	0.036	0.0387	18.5	88
5CuSTO	11		11.9	10.5	11	9.0	0.035	0.0510	17.0	185
10CuSTO	13		9.1	13	13.2	10.2	0.021	0.041	16.2	160
20CuSTO	15		8.2	14	15	7.0	0.013	0.0201	15.7	145

BET Brunauer–Emmett–Teller (isotherm)

^a The standard isotherm used in each case was selected according to [25]

^b α_S surface area

^c Cumulative surface area

^d Cumulative pore volume

^e Total pore volume at $P/P_0 = 0.99$

^f Mean pore radius at the peak of the distribution curves

^g Determined using Eq. 1

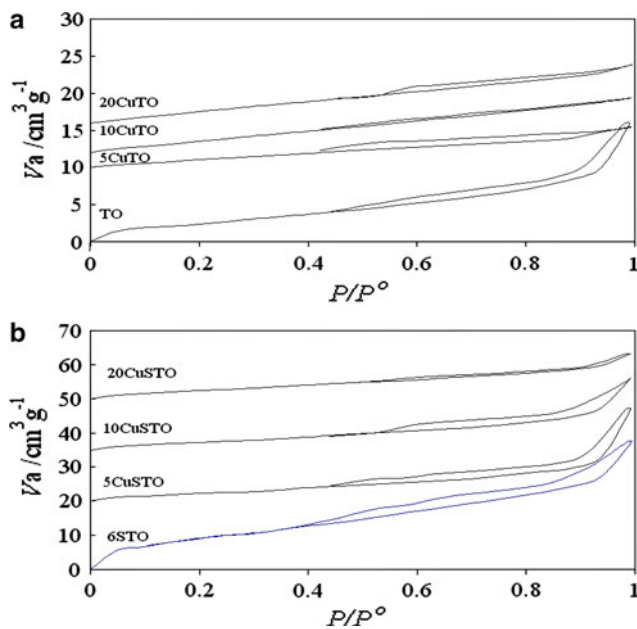


Fig. 3 Nitrogen sorption isotherms for **a** TO and $x\text{CuTO}$ and **b** 6STO and $x\text{CuSTO}$ catalysts; V_a is measured at standard temperature and pressure (STP)

Surface texture

Nitrogen sorption isotherms at 77 K for pure and modified stannia samples are shown in Fig. 3. From these figures, it is clear that all isotherms are belonging to type IV according to BET classification [22] and display hysteresis loops of type H3 according to the International Union of Pure and Applied Chemistry (IUPAC) classification [23]. For all isotherms, the inception point of the hysteresis loops lie at $P/P_0 \approx 0.4$ except for 10CuTO and 20CuTO samples, for which the point appears at higher value of $P/P_0 = 0.5$. This may actually mean that the complete monolayer formation takes place slowly and there is an effective contribution of micropores to the adsorption on the samples.

Data obtained from isotherms and BET plots of the samples under testing are cited in Table 1. From these data it is clear that pure TO sample has low specific surface area ($S_{\text{BET}} = 11 \text{ m}^2 \text{ g}^{-1}$) which agrees with previous data [24]. The addition of sulfate into TO resulted in an increase in the surface area for the sample 6STO to $35 \text{ m}^2 \text{ g}^{-1}$. These data agree with those obtained from XRD results, which are compiled in Table 1, in which the sulfated sample has small crystallite size (88 Å) that affects the specific surface area [7]. Hence, the noticeable increase in the S_{BET} values after sulfation could be attributed to the decrease in the crystallite size rather than any modification in the pore structure of the pure tin oxide. For Cu-modified stannia, there is a slight effect of Cu on the value of specific surface area in which the S_{BET} values are 11, 12, and $14 \text{ m}^2 \text{ g}^{-1}$ for

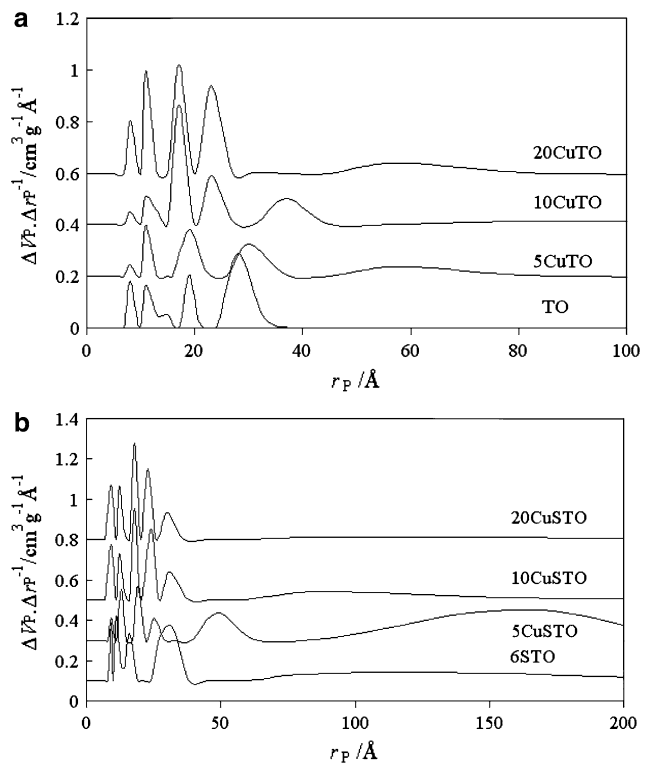


Fig. 4 Pore size distribution curves for **a** TO and $x\text{CuTO}$ and **b** 6STO and $x\text{CuSTO}$ catalysts; r_p true radius and $\Delta V_p / \Delta r_p^{-1}$ ($\text{cm}^3 \text{g}^{-1} \text{\AA}^{-1}$) is the ratio between the volume decrease (ΔV_p) in $\text{cm}^3 \text{g}^{-1}$ and the decrease in pore radius (Δr_p^{-1}) in \AA^{-1}

5CuTO, 10CuTO, and 20CuTO, respectively. These data agree well with the values of XRD crystallite sizes that are 307, 177, and 156 Å for the same samples. On the other hand, for $x\text{CuSTO}$ there is lower effect on the values of surface area. These slight changes in S_{BET} values may be interpreted because of surface pore blockage of stannia during the preparation process with copper acetate [7]. From the data cited in Table 1, the values of V_{Tot} are higher than that of V_{Cum} , which implies the presence of microporosity as well as porosity of complex nature. This is again supported by the higher values of S_{BET} than S_{cum} , where the difference between the two values represents the internal areas inside narrow pores [25].

The pore size distribution (PSD) curves of the samples under study are illustrated in Fig. 4. Examining these curves reveals that the addition of sulfate and modification of stannia by copper cause a development in the porosity, in which all samples are in the micro–meso range. Moreover, any increase in the loading level of Cu can shift the porosity towards lower value. Thus, 10CuSTO shows two peaks at 30 and 90 Å with lower intensity, but the last peak at 170 Å disappeared in the 20CuSTO sample. These results indicate that there is an increase in the proportion of pores with smaller radii. Hence, one could attribute such features in the case of 10CuSTO and 20CuSTO samples to

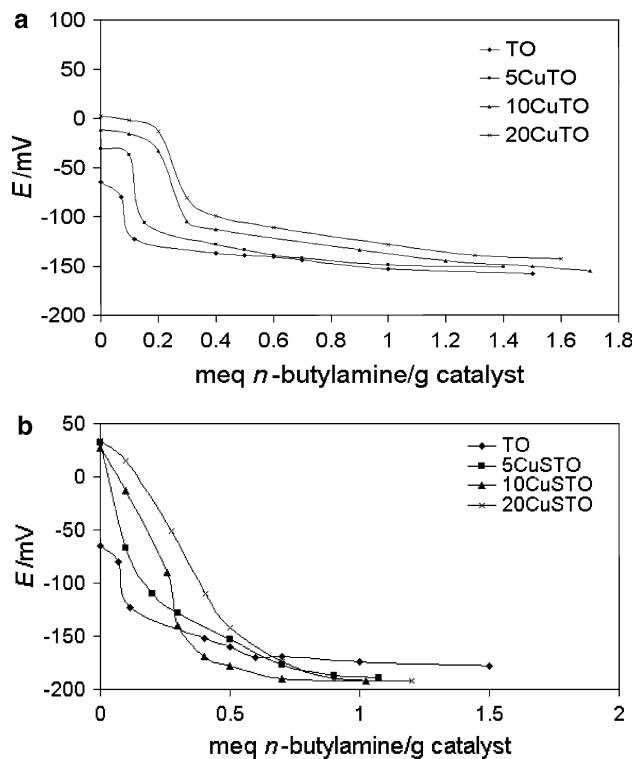


Fig. 5 Potentiometric titration curves for **a** TO and x CuTO and **b** 6STO and x CuSTO catalysts; E is the electrode potential (mV)

the occurrence of pore narrowing because of copper addition and/or creation of new micropores through the evolution of the gases during the calcination process.

Acidity of the catalysts

The total number of acid sites and their relative strength for the catalysts under investigation can be measured by means of a potentiometric titration with 0.1 N *n*-butylamine. To explain the obtained results, it was suggested that the initial electrode potential (E_i) indicates the maximum acid strength of the sites. The value of meq amine/g solid, where the plateau is reached in titration curves (Fig. 5), indicates the total number of acid sites [26–28]. Table 2 shows the potentiometric titration results for all samples. From these results one can conclude that the TO sample has weak acid sites and its maximum strength is equal to -65 mV. The modification with Cu causes an increase in its acidic strength, but remains in the weak range, to become -31 , -12 , and $+2$ mV for the samples 5CuTO, 10CuTO, and 20CuTO, respectively. The addition of sulfate to stannia can increase the acid strength and create strong acid sites on the surface of stannia to become $+47$ mV. For Cu-modified sulfated stannia, their acidic strength became $+50$, $+58$, and $+62$ mV. Thus, addition of copper to sulfated stannia increases the acid strength.

Table 2 Potentiometric titration data for the catalysts

Sample	E_i (mV) = maximum acid strength	No of acid sites (meq g $^{-1}$)
TO	-65	0.11
6STO	$+47$	0.30
5CuTO	-31	0.15
10CuTO	-12	0.30
20CuTO	$+2$	0.40
5CuSTO	$+50$	0.50
10CuSTO	$+58$	0.50
20CuSTO	$+62$	0.70

Table 3 Conversion of phenol and selectivities on some selected catalysts at 333 K

Sample	Phenol conversion (%)	Selectivity (%)			
		CAT	HQ	BQ	RC
TO	0.0	—	—	—	—
6STO	0.0	—	—	—	—
20CuTO	14.8	45.3	52.9	Trace	Trace
20CuSTO	22	21.8	76.4	Trace	Trace

Catalytic activity towards phenol hydroxylation

Hydroxylation of phenols gives three different products, catechol (CAT), hydroquinone (HQ), and resorcinol (RC). Since oxidation of HQ to benzoquinone (BQ) occurs frequently, formation of BQ was also investigated. The results of the catalytic activities using the selected samples (TO, 6STO, 20CuTO, and 20CuSTO) in methanol solvent at 333 K are listed in Table 3. From these data, it is clear that no products are detected when using TO and 6STO samples as catalysts, whereas the Cu-modified samples show a high catalytic activity for hydroxylation of phenol. For the 20CuTO catalyst it is found that the phenol conversion is 14.8% and the reaction tends to give HQ as the main product. By comparing the catalytic performance of Cu-promoted sulfated stannia 20CuSTO with 20CuTO, the phenol conversion on 20CuSTO is 7% higher than that for 20CuTO. Also, the HQ selectivity in the case of 20CuSTO (76.4%) is higher than that of 20CuTO sample (52.9%), which can be interpreted according to the higher acidity of Cu-modified sulfated stannia. This reveals that 20CuSTO is a good catalyst for the hydroxylation of phenol. These results are in agreement with previously obtained data [29, 30]. The product selectivity is also affected by the nature of the solvent [30]: within protic solvents such as methanol, hydroquinone formation prevails over catechol; whereas within an aprotic solvent such as acetone, catechol formation prevails over hydroquinone.

Experimental

Materials

Stannia gel, used as a precursor of sulfated and promoted oxide, was prepared by the method described in the literature [31, 32] by a slow dropwise addition of a 1:1 ammonium hydroxide solution to a 0.3 M aqueous solution of tin(IV) chloride ($\text{SnCl}_4 \cdot 5\text{H}_2\text{O}$, AR grade, BDH, England), with continuous stirring until pH 8 is reached. The white precipitate was left overnight before being filtered and washed thoroughly with 2% $\text{CH}_3\text{COONH}_4$ solution until all chloride was eliminated (silver nitrate test), and then dried at 380 K to constant weight. The dried material was ground to 250-mesh size and kept dry over P_2O_5 . The dry gel thus obtained is denoted TH in the text and was used as a precursor for preparation of SnO_2 and modified stannia catalysts. Pure tin oxide, SnO_2 , was obtained from the dried gel (TH) by calcination at 873 K for 3 h. The resultant oxide, SnO_2 (XRD verified, *vide infra*), is designated TO in the text.

The sulfated stannia sample was prepared by impregnation of $\text{SnO}_2 \cdot x\text{H}_2\text{O}$ (TH) gel with the appropriate amount of 1 M H_2SO_4 solution to obtain 6% SO_4^{2-} by weight. The resultant mixture was dried at 383 K for 24 h, followed by calcination at 873 K for 3 h and the product was designated 6STO.

Sulfated stannia modified with copper was prepared as follows. Three solutions were prepared: the first consisted of 100 cm³ distilled water including calculated amount of TH; the second was 1 M H_2SO_4 solution to obtain 6% SO_4^{2-} by weight; and the third solution contained 50 cm³ distilled water with the calculated amount of copper acetate $\text{Cu}(\text{CH}_3\text{COO})_2 \cdot \text{H}_2\text{O}$. Solution 2 was added to solution 1 dropwise under continuous stirring, followed by the dropwise addition of solution 3 with stirring for 1 h. The mixture of the three solutions was left overnight at room temperature followed by drying at 380 K for 24 h. The dried samples were calcined at 873 K for 3 h. The amount of sulfate for all samples was 6%wt and the amount of Cu metal was calculated to give 5, 10, and 20% by weight. These samples were designated $x\text{CuSTO}$ in the text, where x is the loading of Cu (5, 10, and 20%wt). For the purpose of comparison, copper-modified stannia samples were prepared as above without sulfate addition, to give the samples denoted in the text as 5CuTO, 10CuTO, and 20CuTO.

Apparatus and techniques

Thermal analysis

Both TGA and DTA were performed between room temperature and 1,273 K in a static atmosphere of air by

using a V2-2A DuPont 9900 thermal analyzer. The rate of heating was standardized at 10 K min⁻¹, and small portions (5–15 mg) of the sample were used in TG measurements.

X-ray powder diffractometry

XRD diffractograms were recorded for all samples by using a model JSX-60PA Jeol diffractometer (Tokyo, Japan) and $\text{Cu K}\alpha$ radiation ($\lambda = 1.5418 \text{ \AA}$). The generator was operated at 35 kV and 20 mA. The samples were scanned in the range of $2\theta = 10\text{--}70^\circ$ at a scanning speed of 6° min⁻¹. For identification purposes, diffraction patterns (III°) versus d spacing (Å) were matched with the relevant American Society for Testing Materials (ASTM) standards [33]. The crystallite sizes D of the samples were calculated by using Scherrer's relationship [19]:

$$D = \frac{K\lambda}{\beta \cos \theta} \quad (1)$$

where K is the crystallite shape constant (≈ 1), λ the radiation wavelength, β the line breadth (radians), and θ is the Bragg angle.

Nitrogen sorption measurement

Full nitrogen adsorption/desorption isotherms at 77 K were obtained by using a NOVA 2200 (version 6.10) high-speed gas sorption analyzer (Quantachrome Corp., Boynton Beach, FL, USA). The calcined samples were first degassed at 470 K for 1 h. Twenty-four-point adsorption and desorption isotherms were obtained, from which BET surface areas were derived by using standard and well-established methods [23, 34].

Acidity measurement

The total acidity of the solid samples under investigation was measured by means of potentiometric titration [26, 35]. The solid catalyst (0.1 g) was suspended in 10 cm³ acetonitrile (Merck) and agitated for 4 h. Then, the suspension was titrated with 0.1 N *n*-butylamine in acetonitrile at 0.10 cm³ min⁻¹. The electrode potential (E_i) variation was measured with a SevenMulti, Mettler-Toledo GmbH, Switzerland. We adopted the Cid and Pecci [27] scale of acid strength measurement, defined as follows: $E_i > 100 \text{ mV}$ for very strong sites; $E_i = 0\text{--}100 \text{ mV}$ for strong acid sites; $E_i = -100 \text{ to } 0 \text{ mV}$ weak sites; and finally $E_i < -100 \text{ mV}$ for very weak sites.

Catalytic activity

The catalytic activity of the prepared solid catalysts was studied by using phenol hydroxylation according to the following procedure [9]: the reaction was performed in a 100 cm³ three-necked round-bottom flask, equipped with a magnetic stirrer, a reflux condenser, and a temperature

controllable water bath. In a typical run, the reaction conditions were catalyst/phenol = 20:1 (mg/mmol), phenol/H₂O₂ = 3: 1 (molar ratio), methanol (4 g), $T = 333\text{ K}$. All materials were added to the reactor except H₂O₂; when the mixture was heated to the reaction temperature (333 K) under vigorous stirring, the amount of 30% aqueous H₂O₂ was added to the reactor. The liquid samples were regularly withdrawn with a filtering syringe and analyzed by high-performance liquid chromatography (HPLC, Thermo, C18, 250 × 4.6 mm column, 100% methanol mobile phase, and flow rate 1 cm³ min⁻¹), using UV detectors at 254 nm.

References

1. Askarinejad A, Morsali A (2008) Mater Lett 62:478
2. Askarinejad A, Morsali A (2009) Ultrason Sonochem 16:124
3. Soltanzadeh N, Morsali A (2010) Ultrason Sonochem 17:139
4. Jyothi TM, Sreekumar K, Talawar MB, Mirajkar SP, Rao BS, Sugunan S (2000) Polish J Chem 74:801
5. Song X, Sayari A (1996) Catal Rev Sci Eng 38:329
6. Song X, Reddy KR, Sayari A (1996) J Catal 161:206
7. Khalaf HA (2009) Monatsh Chem 140:669
8. Matsuhashi H, Hino M, Arata K (1988) Chem Lett 1027
9. Wang L, Kong A, Chen B, Ding H, Shan Y, He M (2005) J Mol Catal A Chem 230:143
10. Bruck LG, Gorodskii SN, Zeigarnik AV (1998) J Mol Catal A Chem 131:29
11. Batzill M, Diebold U (2005) Prog Surf Sci 79:47
12. Harrison PG (1989) Chemistry of tin. Blackie, Glasgow
13. Tendulkar SB, Tambe SS, Chandra I, Rao PV, Naik RV, Kulkarni BD (1998) Ind Eng Chem Res 37:2081
14. Magnacca G, Cerrato G, Morterra C, Signoretto M, Somma F, Pinna F (2003) Chem Mater 15:675
15. Mekhemer GAH, Khalaf HA, Mansour SAA, Nohman AKH (2005) Monatsh Chem 136:2007
16. Wang X, Xie Y (2001) React Kinet Catal Lett 72:115
17. Reddy BM, Sreekanth PM, Lakshmanan P, Khan A (2006) J Mol Catal A Chem 244:1
18. Signoretto M, Melada S, Pinna F, Polizzi S, Cerrato G, Morterra C (2005) Micropor Mesopor Mater 81:19
19. Klug HP, Alexander LE (1970) X-ray diffraction procedures. Wiley, New York, p 490
20. Khder AS, El-Sharkawy EA, El-Hakam SA, Ahmed AI (2008) Catal Commun 9:769
21. Jogalekar AY, Jaiswal RG, Jayaram RV (1998) J Chem Technol Biotechnol 71:234
22. Brunauer S, Emmett PH, Teller T (1938) J Am Chem Soc 60:309
23. Sing KSW, Everett DH, Haul RAW, Moscou L, Pierotti RA, Rouquerol J, Siemieniewska T (1985) Pure Appl Chem 57:603
24. Harrison P, Guest A (1989) J Chem Soc Faraday Trans 85:1897
25. Khalaf HA (2005) PhD thesis, Minia Univ, Egypt
26. El-Sharkawy EA, Khder AS, Ahmed AI (2007) Micropor Mesopor Mater 102:128
27. Cid R, Pecci G (1985) J Appl Catal A Gen 14:15
28. Sharma P, Vyas S, Patel A (2004) J Mol Catal 214:281
29. Thangaraj A, Kumar R, Ratnasamy P (1991) J Catal 131:294
30. Tuel A, Khouzami SM, Ben Yaarit Y, Naccache CM (1991) J Mol Catal 68:45
31. Matsuhashi H, Miyazaki H, Arata K (2001) Chem Lett 452
32. Matsuhashi H, Miyazaki H, Kawamura Y, Nakamura H, Arata K (2001) Chem Mater 13:3038
33. Joint Committee on Powder Diffraction Standards (1978) X-ray powder data file. American Society for Testing Materials, Pennsylvania
34. Webb PA, Orr C (1997) Analytical methods in fine particle technology. Micromeritics, Norcross, GA
35. Rao KN, Reddy KM, Lingaiah N, Suryanarayana I, Prasad PS (2006) J Appl Catal A Gen 300:139